Impact of USGS Vegetation Map on GCM Simulations over the United States

M. J. Fennessy; Y. Xue

Ecological Applications, Vol. 7, No. 1 (Feb., 1997), 22-33.

Stable URL:
http://links.jstor.org/sici?sici=1051-0761%28199702%297%3A1%3C22%3AIOUVMO%3E2.0.CO%3B2-V

Ecological Applications is currently published by The Ecological Society of America.

Ecological Applications, 7(1), 1997, pp. 22–33

IMPACT OF USGS VEGETATION MAP ON GCM SIMULATIONS OVER THE UNITED STATES

M. J. FENNESSY AND Y. XUE

Center for Ocean–Land–Atmosphere Studies, 4041 Powder Mill Road, Suite 302, Calverton, Maryland 20705 USA

Abstract. A global atmospheric general circulation model (GCM) coupled with a biosphere model (SSiB, simplified simple biosphere model) was used to study the impact of vegetation on simulations over the United States during summer. Ensembles of 90-d integrations were performed from early June initial conditions with different vegetation maps and different biophysical characteristics. Monthly and seasonal mean differences among these ensembles were analyzed.

Incorporation of a new SiB vegetation map produced from the latest available data by the U.S. Geological Survey's EROS (Earth Resources Observation Systems) Data Center has a significant impact on monthly and seasonal simulations of evaporation, surface air temperature, and precipitation over some regions of the United States. The impact is greater over the western half of the United States than over the eastern half, where moisture convergence plays a stronger role in the hydrological cycle.

Systematic errors in the model simulations appear to be related to the use of a single crop vegetation type in SiB (simple biosphere model). Replacing the crops over the United States with broadleaf deciduous trees reduces the systematic errors. It appears that the strong seasonality of the SiB crop vegetation type makes it an unsuitable representative for crops in general. The importance of vegetation specification in monthly and seasonal predictions is emphasized.

Key words: atmospheric general circulation model; biosphere modeling; General Circulation Model (GCM) systematic errors; monthly and seasonal precipitation; Simple Biosphere Model (SiB) vegetation map; U.S. Geological Survey vegetation map; vegetation impact; vegetation parameters.

INTRODUCTION

Coupled biosphere–atmosphere modeling, which began during the 1980s, consists of coupling a sophisticated land surface–atmospheric interaction model to a multilayer atmospheric model, usually a general circulation model (GCM). The development of these coupled models was motivated by improvements in the parameterizations in both land surface process schemes and GCMs, the increasing spatial resolution of GCMs, and the needs of global climate change research. The need for such coupled models was demonstrated by a wide variety of GCM sensitivity studies, which showed the importance of land surface properties in controlling water and energy exchanges at the land surface. These sensitivity studies generally investigated the response of the simulated atmosphere to one of the key surface properties, most prominently albedo (e.g., Charney et al. 1977, Sud and Fennessy 1982), soil wetness (e.g., Walker and Rowntree 1977, Shukla and Mintz 1982) and surface roughness (e.g., Sud and Smith 1985). For a review of these studies see Mintz (1984). While these studies clearly showed the importance of these individual land surface properties, they also revealed the inconsistencies inherent in independently altering just one of the important surface properties, which are linked together and moderated by vegetation (Sellers et al. 1986).

Two of the most prominent land surface–atmosphere interaction models are the biosphere–atmosphere–transfer scheme (BATS; Dickinson et al. 1986) and the simple biosphere model (SiB; Sellers et al. 1986). Using these models coupled to GCMs, studies have been conducted on Amazonian deforestation and Sahel desertification (Dickinson and Henderson-Sellers 1988, Xue and Shukla 1993).

SiB is a biophysically based model of land surface–atmosphere interactions. It is intended to realistically simulate the biospheric processes that control surface fluxes of importance to regional and global climate studies. SiB attempts to provide an accurate description of the diurnally varying surface flux components and radiation transfers at the surface. It accounts for vegetation effects such as precipitation–interception loss and the soil and plant resistances to evapotranspiration, sensible heat flux, and momentum flux. In this study, a simplified version of SiB (SSiB; Xue et al. 1991)

Manuscript received 2 December 1994; revised and accepted 30 October 1995; final version received 22 May 1995. For reprints of this Invited Feature, see footnote 1, page 1.

TABLE 1. U.S. region SiB vegetation types, vegetation cover fraction (VC), leaf area index (LAI), albedo (ALB), total soil depth (TSD), and surface roughness (Z_0).

Number	SiB vegetation type	VC	LAI†	ALB†	TSD (m)	Z_0 (m)
2	broadleaf deciduous trees	0.75	5.11	0.13	3.50	1.04
3	broadleaf and needleleaf trees	0.75	6.36	0.11	3.50	0.56
4	needleleaf evergreen trees	0.75	7.87	0.10	3.50	1.07
7	grassland	0.90	3.80	0.20	1.49	0.08
8	broadleaf shrubs with perennial ground cover	0.10	0.44	0.20	1.49	0.22
9	broadleaf shrubs with bare soil	0.10	0.21	0.30	1.49	0.06
11	bare soil	0.00	0.00	0.32	0.49	0.01
12	winter wheat and broadleaf deciduous trees‡	0.32	1.37	0.13	1.49	0.49

† Three-month mean values.
‡ Average over 30° N to 50° N.

coupled to the Center for Ocean–Land–Atmosphere Studies (COLA) GCM was used in numerical experiments.

For a coupled biosphere–GCM model, it is critical to have information regarding the characteristics and spatial distribution of the Earth's vegetation cover. The First International Conference/Workshop on Integrating Geographic Information Systems (GIS) and Environmental Modeling successfully brought together scientists from a broad range of environmental modeling specialties, as well as persons involved in developing or using geoprocessing technologies (Goodchild et al. 1993). One of the goals of the conference was to convey the global climate modeling requirements to the data and geoprocessing community. A number of models, including SiB (Xue and Sellers 1993), were introduced at the conference. Following the conference, a vegetation map, which consists of the 12 SiB vegetation types over the conterminous U.S., was produced by the Earth Resources Observation Systems (EROS) Data Center, U.S. Geological Survey (USGS). We will refer to it as the USGS SiB map in this paper. The USGS SiB map is based on the land cover characteristics database for the conterminous U.S. (Loveland et al. 1991), which has >100 vegetation types and a horizontal resolution of 1 km.

SiB vegetation types include tall vegetation, short vegetation, arable crops, and desert (Dorman and Sellers 1989). A summary of some of the key parameters for the SiB vegetation types that occur in the conterminous U.S. is given in Table 1. In the GCM, every grid point is assigned one vegetation type. For previous experiments, the main sources for the distribution of the world vegetation types were the physiognomic classification of Kuchler (1983) and the land use database of Matthews (1984), which were used to form the original SiB vegetation map, hereafter referred to as the OLD SiB map. It has been found that there are a number of places where Kuchler's classifications (and thus the OLD SiB map) differ from the current land surface conditions. We compare the differences between the USGS SiB map and the OLD SiB map in this paper and use both in numerical experiments designed to test the impact of the vegetation map on seasonal simulations. The results of these experiments revealed model systematic errors, which appeared to be correlated with the local SiB vegetation type. Further experiments were done to investigate this possibility.

METHODS

Model description

Atmospheric general circulation model.—An atmospheric general circulation model (GCM) simulates the three-dimensional evolution of the atmosphere by computationally solving the equations that govern the dynamics and physics of the atmosphere. In a spectral GCM such as the COLA GCM, the prognostic computations are done in the spectral domain and the physical processes are computed on a grid (≈1.8° latitude × 2.8° longitude).

The COLA GCM is based on a modified version of the National Meteorological Center global spectral model with rhomboidal truncation at zonal wave number 40 (Sela 1980, Kinter et al. 1988, Fennessy et al. 1994). The model is separated into 18 vertical layers. The parameterizations for physical processes include: (1) an efficient radiation scheme, which resolves the diurnal cycle and includes terrestrial radiative heating (Harshvardhan et al. 1987), and solar radiative heating (Lacis and Hansen 1974, modified by Davies 1982); an interactive cloud scheme, which is similar to the one developed by Slingo [1987], was incorporated into the GCM for the radiation calculations [Hou 1990]; (2) the level 2.0 second-order turbulence closure scheme of Mellor and Yamada (1982) for subgrid-scale exchanges of heat, momentum, and moisture; (3) a modified Kuo scheme for convection (Kuo 1965, Anthes 1977), shallow convection (Tiedke 1984), and large-scale condensation; (4) a gravity-wave drag parameterization, which follows that of Alpert et al. (1988).

Simplified SiB model (SSiB).—The SSiB model (Xue et al. 1991) is used to model the surface layer in the COLA GCM. SSiB has three soil layers and one canopy layer, and eight prognostic variables: soil wetness in the three soil layers; temperature at the canopy, ground

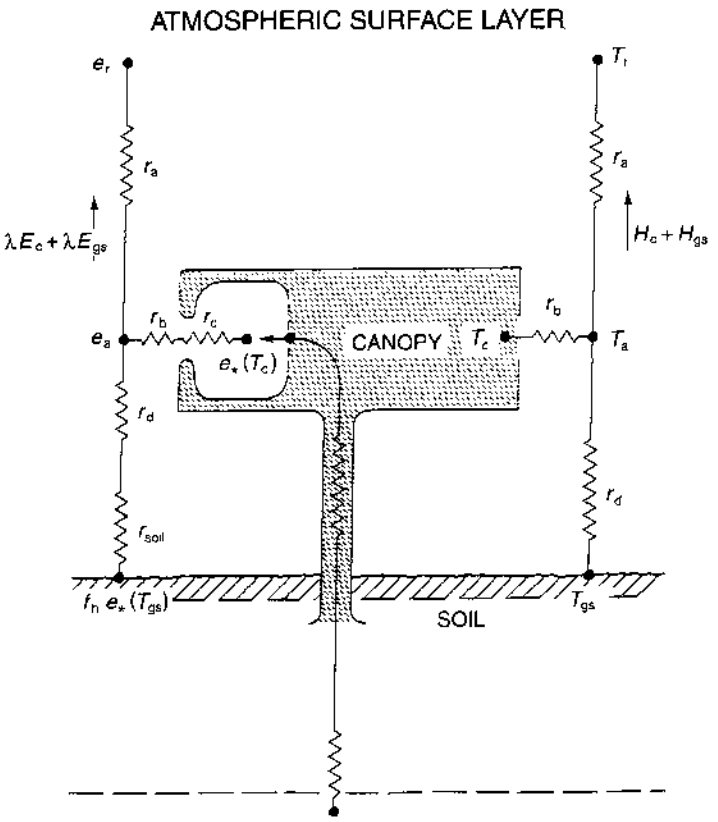

FIG. 1. Schematic diagram of simplified SiB (SSiB). The transfer pathways for latent and sensible heat flux are shown on the left- and right-hand sides of the diagram, respectively. T_r is the air temperature at reference height, T_c the canopy temperature, T_a the air temperature within the canopy space, T_{gs} the ground surface temperature, r_a the aerodynamic resistance between canopy air space and reference height, r_b the bulk boundary layer resistance, r_c the bulk stomatal resistance, r_d aerodynamic resistance between canopy air space and ground, and r_{soil} the bare soil surface resistance. H_c and H_{gs} are the sensible heat flux from canopy and ground, respectively; E_c and E_{gs} are the latent heat fluxes from canopy and ground, respectively; e_r and e_a are the water vapor pressures at the reference height and the canopy air space, respectively; $e_*(T)$ is the saturation water vapor pressure at temperature T; f_h is relative humidity within the pore space of surface soil layer; and λ is the latent heat of evaporation.

surface, and deep soil layers; water stored on the canopy; and snow stored on the ground. A schematic diagram of SSiB is shown in Fig. 1.

The vegetation–soil layer affects the radiative transfer at the surface, the surface energy partition into sensible heat flux and latent heat flux, and the momentum flux. A biosphere model attempts to describe the biophysical controls on these exchanges by modeling the vegetation itself so that the exchange processes are mutually consistent. There are three major parts in SSiB: calculations of radiative transfer at the surface, stomatal resistances, and aerodynamic resistances.

In the radiative transfer parameterization, the optical and geometric properties of the leaves and stems and the optical properties of the soil are considered to calculate the surface albedo and the alteration of photosynthetically active radiation (PAR) down through the canopy. Since the variation of the albedo with these variables is quite regular, a quadratic equation is used to calculate the albedo diurnal variation. The coefficients of the quadratic equation depend on the vegetation type. For a specific vegetation type the albedo is also a function of the solar zenith angle and snow cover.

The resistance to the transfer of water vapor from the canopy and upper soil layer to the adjacent exterior air includes canopy resistance, r_c, and soil surface resistance, r_{soil}. The results of Camilo and Gurney (1986) were used to curve-fit a simple relationship between soil surface resistance and wetness of the upper 0.5 cm of the soil. The parameterization of the stomatal resistance in SiB was based on the work of Jarvis (1976). An analytic solution for the bulk stomatal resistance was introduced by Sellers (1985). Three stress terms are included in this scheme, which describes the dependence on the atmospheric temperature, the leaf water potential, and the vapor pressure deficit. An empirical equation between the soil moisture and the adjustment factor of the stomatal resistances was developed by Xue et al. (1991).

There are three aerodynamic resistances in SiB: the resistance between the soil surface and the canopy air space, r_d; the resistance between the canopy and the canopy air space, r_b; and the resistance between the canopy air space and the reference height, r_a (Fig. 1). Eddy diffusion was used to calculate all three resistances. The eddy fluxes were assumed to be constant below and above the canopy; within the canopy K theory was applied. The parameterization of the resistance between the reference height and top of canopy was based upon the equations of Paulson (1970) and Businger et al. (1971). Since the full set of equations were too time-consuming to apply directly in a GCM, a linear relationship between the Richardson number and aerodynamic resistance was developed (Xue et al.

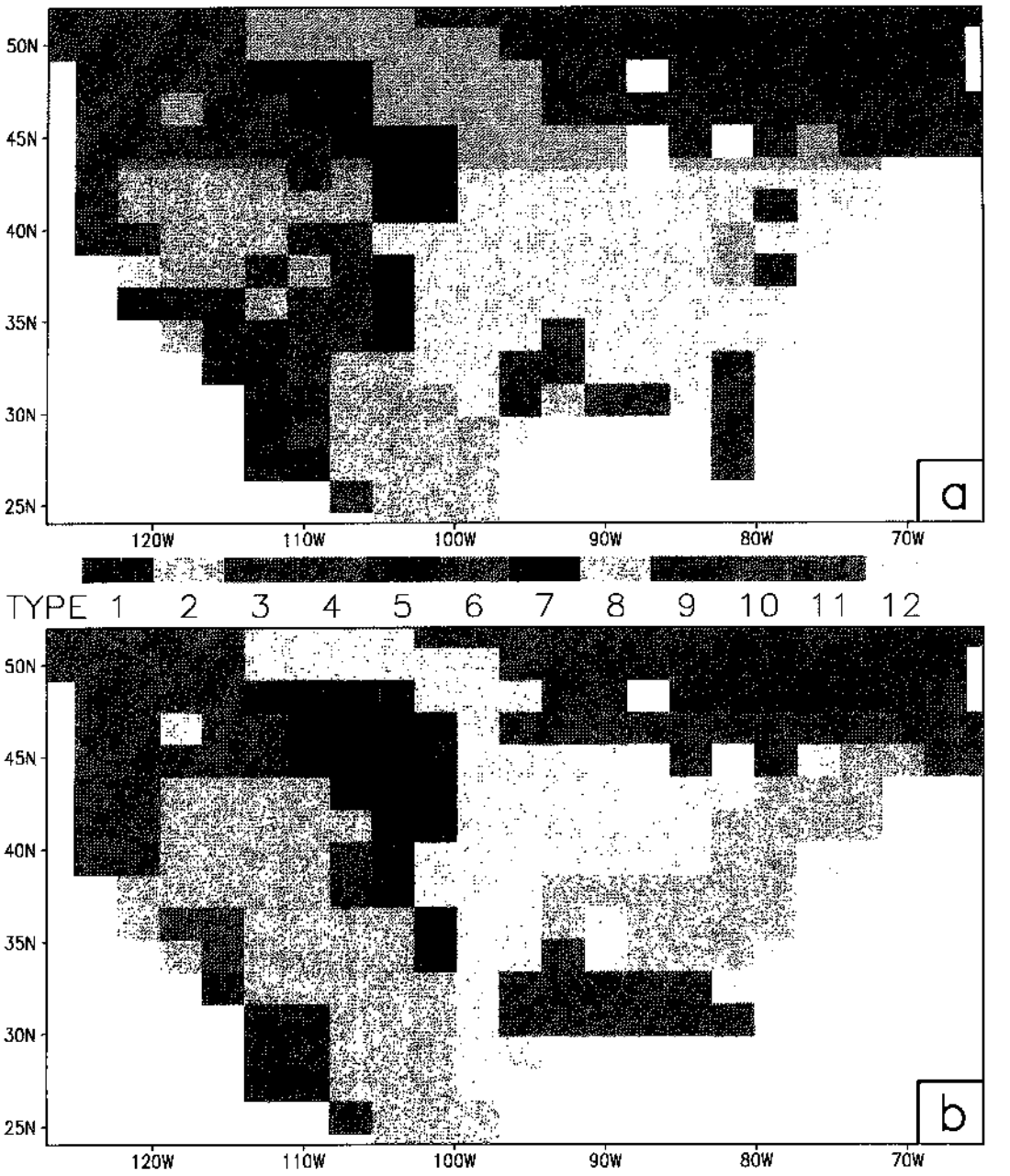

PLATE 1. Vegetation types for (a) OLD SiB vegetation map and (b) USGS SiB Vegetation map. Types are: 2—broadleaf deciduous trees, 3—broadleaf and needleleaf trees, 4—needleleaf evergreen trees, 7—grassland, 8—broadleaf shrubs with perennial ground cover, 9—broadleaf shrubs with bare soil, 11—bare soil, 12—winter wheat and broadleaf deciduous trees.

1991). The linear equations were able to reproduce the results from the full set of equations satisfactorily.

Vegetation map.—SiB uses a data set that describes each vegetation type's soil and vegetation characteristics in some detail. For each GCM gaussian grid box ($\approx$1.8° latitude $\times$ 2.8° longitude), the dominant vegetation type is specified from among the 12 SiB vegetation types in the 1° $\times$ 1° SiB vegetation map. Here we show the SiB vegetation maps on the GCM gaussian grid, which are used during the integrations. The OLD SiB vegetation map for the United States and contiguous area is shown in Plate 1a and the USGS SiB vegetation map is shown in Plate 1b. Values of some key parameters for the vegetation types occurring in the conterminous U.S. are shown in Table 1. In order to emphasize the differences between the OLD SiB map and the USGS SiB map, for grid boxes where the vegetation type differs between the two, the old types are

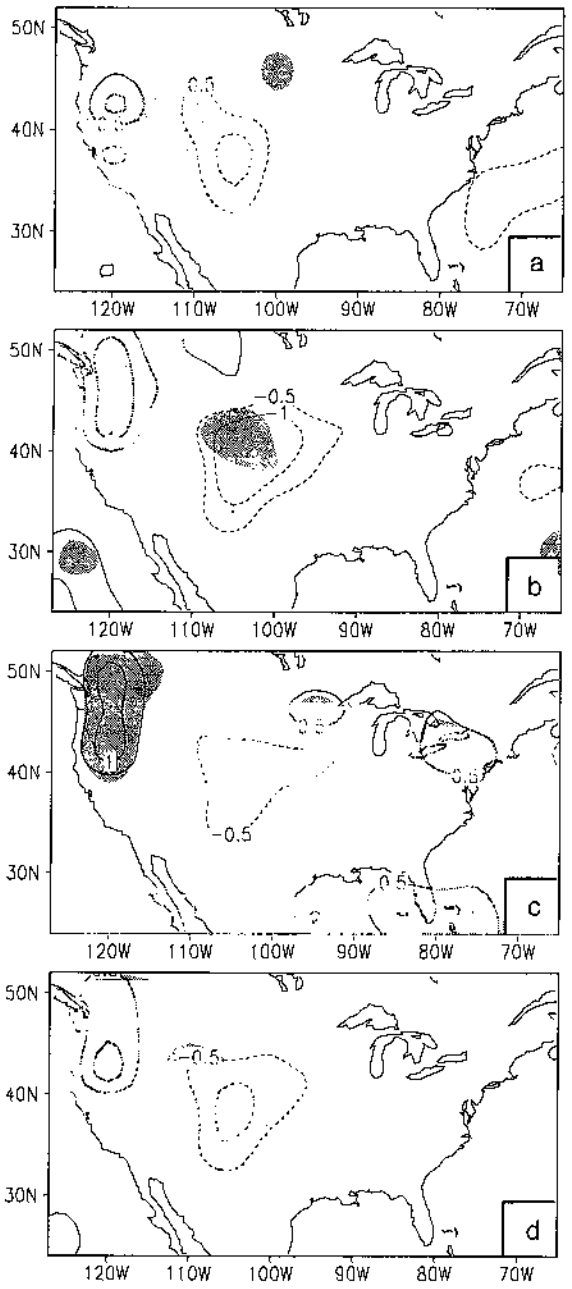

FIG. 2. USGS SiB map minus OLD SiB map ensemble difference in evaporation for (a) June, (b) July, (c) August, and (d) JJA (June-July-August mean). Contours show differences in mm/d. Dashed contours are negative. Areas with statistically significant differences are denoted by shading.

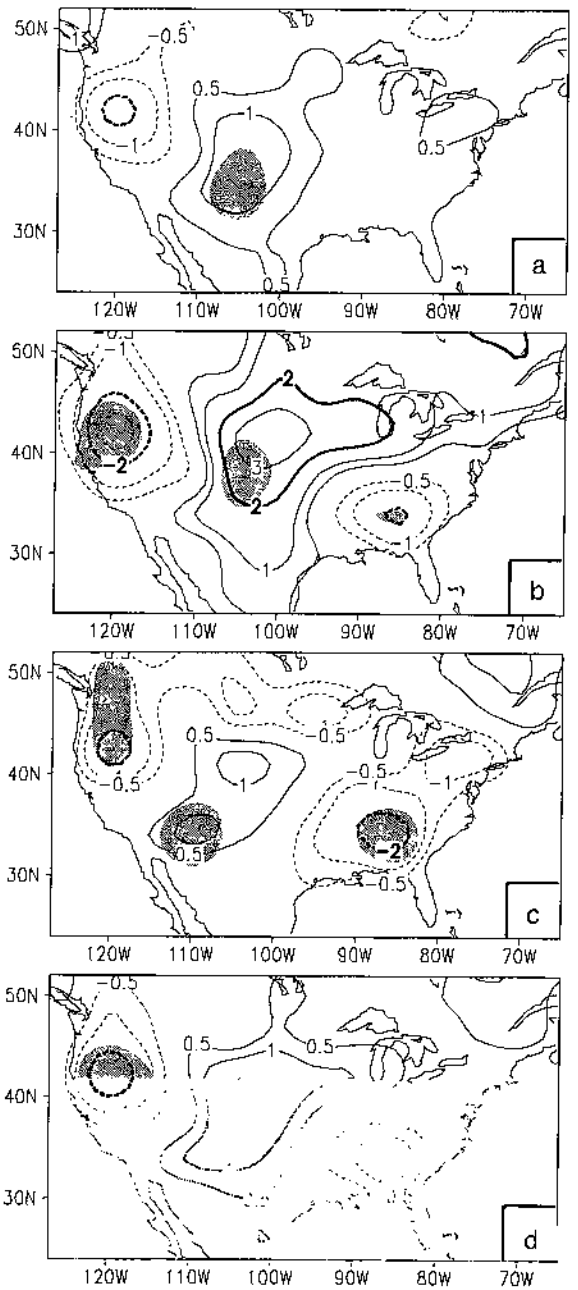

FIG. 3. USGS SiB map minus OLD SiB map ensemble difference in surface air temperature for (a) June, (b) July, (c) August, and (d) JJA (June-July-August mean). Contours show differences in °C. Dashed contours are negative. Areas with statistically significant differences are denoted by shading.

shown in Plate 2a and the new types are shown in Plate 2b.

In the USGS SiB map (Fig. 2b), the crop area (type 12) is substantially reduced (Fig. 3a) relative to that in the OLD SiB map (Fig. 2a). The crops were replaced by broadleaf deciduous trees (type 2) and needleleaf evergreen trees (type 4) in the eastern U.S., and replaced by grass (type 7) in the northern Rocky Mountains area (Plate 2b). To the west of the Rocky Mountains, needleleaf evergreen trees (type 4) in the OLD SiB map were replaced by shrubs with ground cover (type 8). In northern California and southern Oregon shrubs with ground cover (type 8) were replaced with needleleaf evergreen trees (type 4). The southern Nevada desert is appropriately characterized as bare soil

(type 11) in the USGS SiB map instead of as shrubs (type 9) in the OLD SiB map.

Experimental design

Two sets of numerical experiments were conducted. In the first set of experiments, the impact of the USGS SiB vegetation map on the model simulations was tested. The COLA GCM was integrated for 90 d from three different atmospheric conditions observed in early June using the OLD SiB vegetation map. These three integrations were then repeated identically, except that the USGS SiB map was used instead of the OLD SiB map. The difference between a given OLD SiB map integration and the corresponding USGS SiB map integration will consist of the signal forced by the vegetation map difference and noise related to the internal variability inherent in the GCM simulations. Three pairs of integrations were done to help distinguish the vegetation map signal from this noise. The consistent signal among three individual difference fields is reflected by a t test statistic, which is computed from the six individual integrations. This consistent signal is assumed to be forced by the vegetation map difference. Implicit in this assumption is the assumption that any model "climate drift" is common to both the control (OLD SiB map) and anomaly (USGS SiB map) integrations, and will therefore not impact the signal in the anomaly minus control difference.

The dates of the observed atmospheric initial conditions used were 1 June 1987, 1 June 1988, and 1 June 1993. Among the three cases, 1988 was a very dry year in the U.S., 1993 was a very wet year, and 1987 was relatively normal. As the USGS SiB map covers only the conterminous United States (hereafter, U.S.), outside this region the OLD SiB map is used in all the integrations. Observed sea surface temperature (Reynolds 1988) was used in all the integrations. The differences between the three integrations done with the OLD SiB map and the three integrations done with the USGS SiB map were analyzed to determine the impact of the vegetation map differences.

The results from the first experiment revealed that there were systematic errors in the simulated surface temperature and precipitation over the U.S., which mainly occurred over the area assigned the SiB crop vegetation type (type 12). In SiB all crop areas are represented with the phenological, biophysical, and crop calendar characteristics of winter wheat, mixed with 8% broadleaf deciduous trees. It is possible that the application of these unique winter wheat characteristics to all crop areas in SiB constitutes a misrepresentation of sufficient enough magnitude to produce or contribute to the systematic errors found in the first experiment. However, it is also possible that the systematic errors are merely coincidental with the crop area, and are unrelated to the local vegetation specification. Therefore, to investigate whether the use of the SiB crop vegetation type is related to these systematic errors, an additional ensemble of three integrations was done in which the crops in the USGS SiB vegetation map were replaced by broadleaf deciduous trees (type 2). The differences between these three integrations (hereafter TREE integrations), and the three integrations done with the USGS SiB map, are analyzed to determine the impact of replacing the SiB crop vegetation type over the U.S. with the SiB broadleaf deciduous tree vegetation type.

Results and Discussion

Impact of USGS SiB vegetation map

The differences between the three OLD SiB vegetation map integrations and the three USGS SiB map integrations are analyzed to determine the impact of the vegetation map on the monthly and seasonal simulations. The only difference between the two sets of integrations is in the vegetation map used, which is different only over the conterminous U.S. In a global atmospheric GCM, which includes the chaotic nonlinear dynamics inherent in the atmosphere, it is possible that forcing from remote regions not directly related to the U.S. vegetation map may have an impact on the U.S. region. It is also possible that remote teleconnections (signals) could be forced by the U.S. vegetation map differences. We have examined the differences between these two sets (OLD SiB map, USGS SiB map) of integrations over the globe, and did not find any consistent remote patterns suggestive of either teleconnections or of remote forcing impacting upon the conterminous U.S. region. Thus, the analysis presented here will focus on the local response to the vegetation map differences over the U.S. Furthermore, the analysis will focus on the important simulated fields most affected, namely the evaporation, surface air temperature, and precipitation.

We have examined the monthly and seasonal mean differences between the OLD SiB map integrations and the USGS SiB map integrations for each of the years (1987, 1988, and 1993), and have found very consistent signals among them. For the sake of brevity, we will show only ensemble differences averaged over the 3 yr. However, the signals we will discuss are local to the forcing (regions of vegetation map differences), and occurred in each of the 3 yr. On the ensemble difference maps we will denote the regions where this signal was deemed significant by a t test, which in these experiments reflects very well the regions where a consistent signal occurred in the difference maps for the individual years. The t test in each case was calculated from the same six individual means (three control, three anomaly) used to form the ensemble difference presented.

The USGS SiB map minus the OLD SiB map ensemble mean difference in evaporation is shown for June, July, August, and the 3-mo June-July-August

mean (JJA) in Fig. 2a–d, respectively. The shaded areas in Fig. 2 and the remaining figures denote where the ensemble mean difference was significant at the 95% confidence level, as determined by a t test. Two regions have significant differences in evaporation in each of the 3 mo as well as in the seasonal mean. Positive evaporation differences of 0.5–1 mm/d occur in the northwestern U.S., in the vicinity where evergreen trees (type 4) in the USGS SiB map replaced shrubs with ground cover (type 8) in the OLD SiB map (Plate 2a, b). Negative evaporation differences of 0.5–1 mm/d occur in the midwestern U.S. where crops (type 12) in the OLD SiB map were replaced by ground cover (type 7), and evergreen trees (type 4) in the OLD SiB map were replaced by shrubs with ground cover (type 8). These areas of significant differences are consistent with the local vegetation changes, with increased (decreased) evaporation corresponding to areas with increased (decreased) vegetation cover, leaf area index, total soil depth, and surface roughness (Table 1).

The USGS SiB map minus the OLD SiB map ensemble difference in surface air temperature for June, July, August, and JJA is shown in Fig. 3a–d, respectively. Significant negative (positive) surface temperature differences occur over the previously noted regions of significant positive (negative) evaporation differences in northwestern (midwestern) U.S., as might be expected from surface energy balance considerations. In addition, a region of marginally significant negative surface temperature differences occurs over the southeastern U.S., in the vicinity where crops (type 12) were replaced by trees (types 2 and 4).

The USGS SiB map minus OLD SiB map ensemble difference in precipitation for June, July, August, and JJA is shown in Fig. 4a–d, respectively. The precipitation differences are in general more variable from month to month and less statistically significant than either the evaporation or surface temperature differences. However, persistent positive precipitation differences occur over the region of positive evaporation and negative surface temperature differences in the northwest; and persistent negative precipitation differences occur over the region of negative evaporation and positive surface temperature differences in the midwest. Both of these precipitation differences are more significant in the JJA seasonal mean than in the monthly means. The negative precipitation difference over the midwest extends to the east of the midwestern negative evaporation difference in both the monthly and seasonal means (Fig. 2a–d). The precipitation reduction over the eastern U.S. is consistent with the significant reduction in the vertically averaged moisture flux convergence, which occurred over this area in the USGS SiB map ensemble (not shown).

In contrast to the simulated differences over the western half of the country, it is somewhat surprising that more coherent differences did not occur over the eastern U.S. where much of the crop vegetation type in the OLD SiB map was replaced by trees in the USGS SiB map. Differences did occur between the individual pairs of the ensemble, but they were of relatively small magnitude and were highly variable from pair to pair. The significant evaporation differences that occurred over the western half of the U.S. did not occur over the eastern half. This is due to the strong zonal gradient

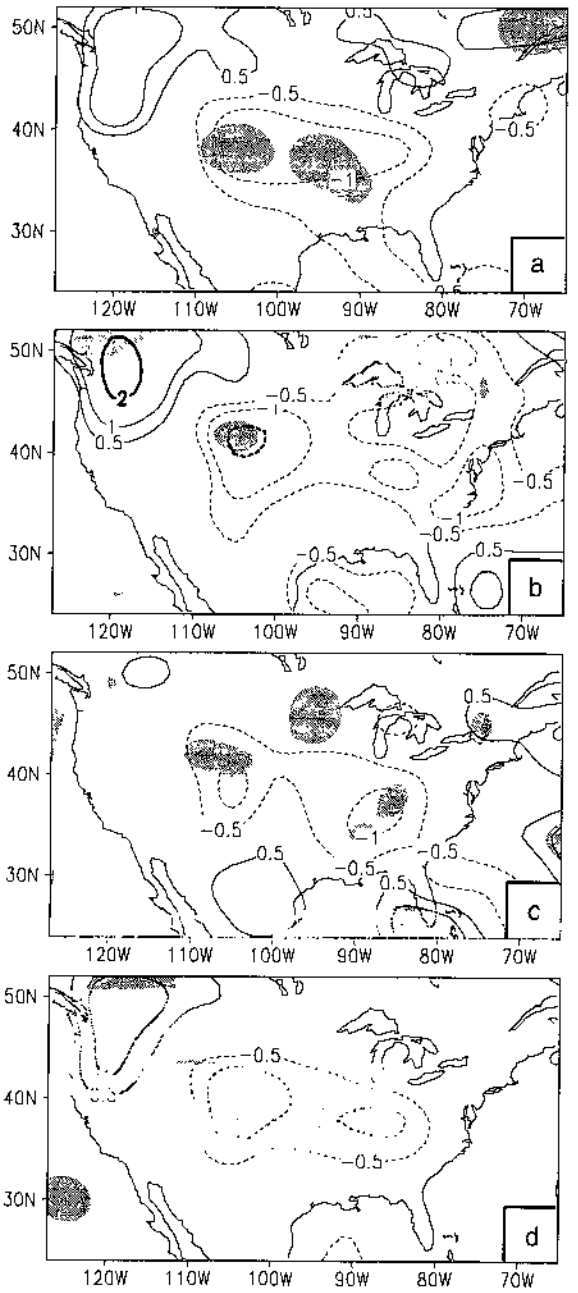

FIG. 4. USGS SiB map minus OLD SiB map ensemble difference in precipitation for (a) June, (b) July, (c) August, and (d) JJA (June-July-August mean). Contours show differences in mm/d. Dashed contours are negative. Areas with statistically significant differences are denoted by shading.

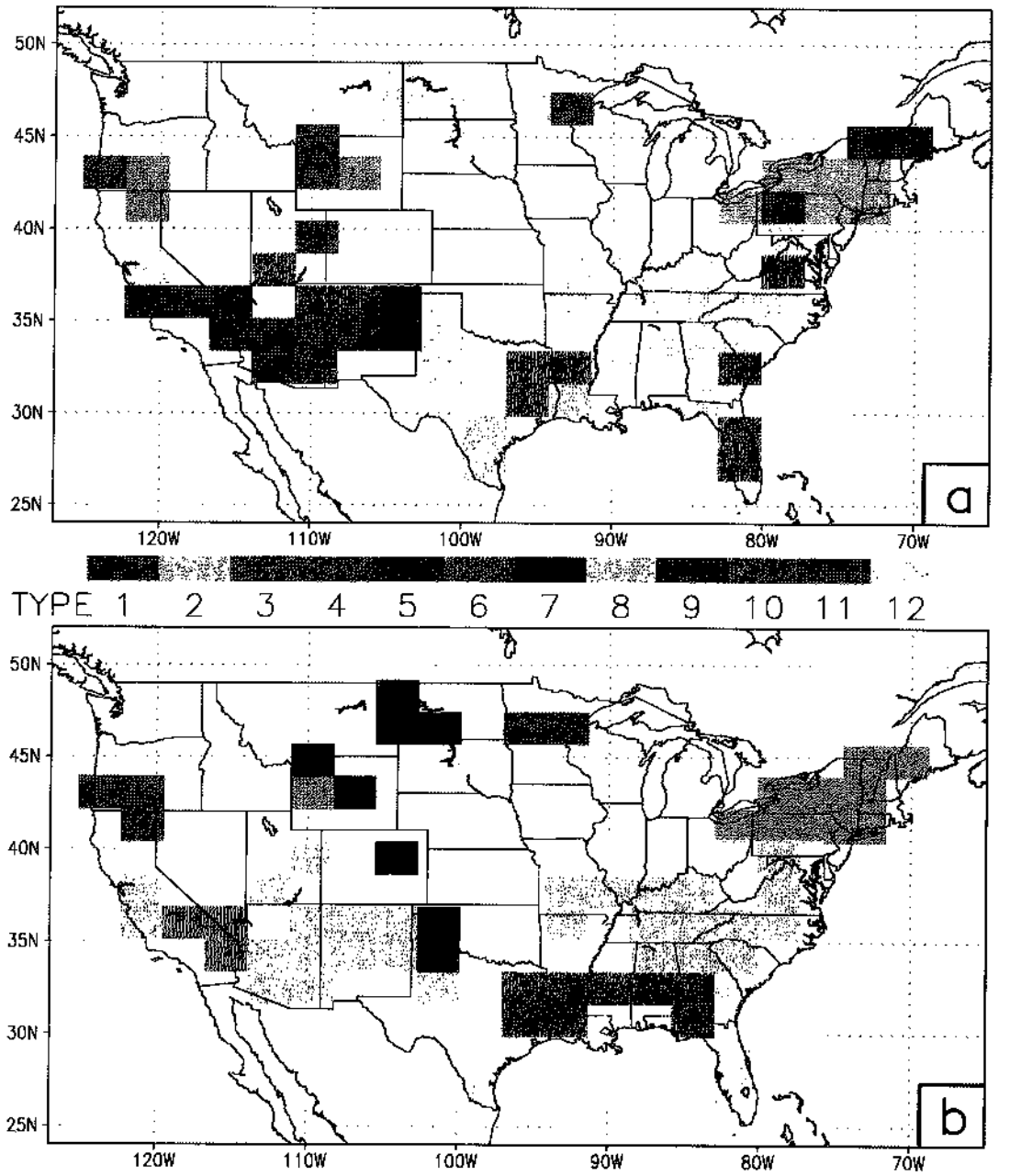

PLATE 2. Vegetation types for model grid boxes where OLD SiB vegetation map and USGS SiB vegetation map differ for (a) OLD SiB vegetation map and (b) USGS SiB vegetation map. Types are as in Fig. 2.

of the mean soil wetness field (not shown). The model is initialized with a climatological soil wetness field, which is at or near saturated values across the eastern U.S. on 1 June. Furthermore, although the soil wetness is prognostic, the eastern U.S. remains near saturated values for most of the summer integrations. Under saturated or near saturated conditions, the vegetation impact is less important.

In the western and midwestern U.S., the vegetation differences lead to evaporation differences that are related to the surface temperature differences (through the surface energy balance) and the precipitation differences (through the atmospheric moisture budget). Thus, in this region increasing (decreasing) the vegetation cover fraction, leaf area index, soil depth, and surface roughness leads to increased (decreased) evaporation and precipitation, and decreased (increased) surface air temperature.

No significant differences between the two ensembles occurred in the upper level circulation fields over

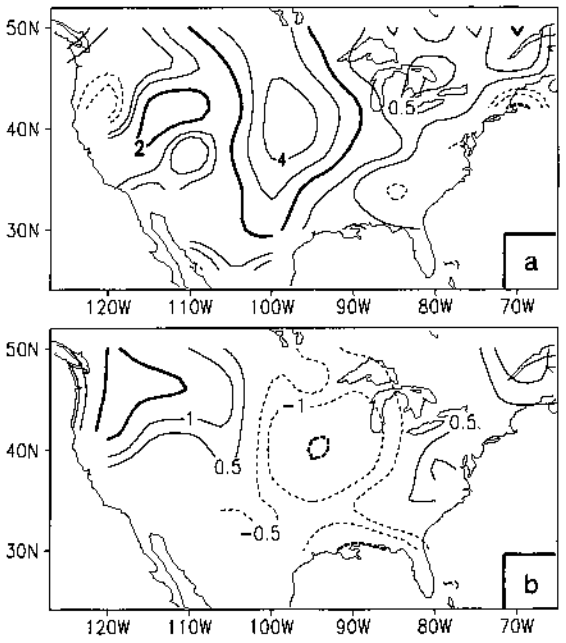

FIG. 5. USGS SiB map ensemble minus observed JJA (June-July-August) mean error in (a) surface air temperature (contours show differences in °C), and (b) precipitation (contours show differences in mm/d). Dashed contours are negative.

the U.S. or other regions of the globe. This supports our contention that the differences noted above are locally forced by the vegetation map differences and are not due to remote teleconnections, which are believed to occur at upper levels of the atmosphere. It also suggests that remote teleconnections are not being forced by the U.S. vegetation map differences.

Impact of replacing crops with trees

As discussed in *Methods: Experimental design*, analysis of the results of the first experiment led to the question of whether the use of the SiB crop vegetation type was related to model systematic errors over a portion of the conterminous U.S. Thus, an experiment was done to determine the impact of replacing SiB crops (type 12) in the USGS SiB map with SiB broadleaf deciduous trees (type 2), which normally comprise 8% of the area of a grid box with SiB vegetation type 12. This experiment was motivated by the similarity of the spatial extent of some of the model summer systematic errors and the extent of the SiB crop vegetation type over the U.S. The large area of type 12 vegetation covering much of the central and eastern U.S. in the USGS SiB map (Fig. 2b) is similar in extent to the region of positive surface temperature errors and negative precipitation errors in the USGS SiB map ensemble, shown in Fig. 5a and b, respectively. Errors of similar spatial extent and magnitude have occurred in other boreal summer ensembles done with the COLA GCM using the OLD SiB vegetation map, in which the spatial extent of vegetation type 12 was even larger (not shown). If the model systematic errors are related to the use of the SiB crop vegetation type, it may be that the parameters used for the SiB crop vegetation type may need to be revised, or that multiple crop vegetation types are required to accurately model the variety of crops found in the conterminous U.S.

The errors shown in Fig. 5 were formed by subtracting the JJA mean observations calculated from the National Meteorological Center (NMC), Climate Analysis Center (CAC), Climate Anomaly Monitoring System station data archive (CAMS, Ropelewski et al. 1985) from the JJA mean of the previously discussed USGS SiB map ensemble. The surface temperature errors include a correction for the difference in elevation between the model grid boxes and the observing stations. The observing stations tend to be situated in valleys, which are generally at a lower elevation than the mean elevation over a model grid box, which is used by the GCM. To account for this difference a lapse rate of 6.5°C/km was used to correct the GCM surface air temperature for the difference between the grid box elevation and the mean elevation of the observing stations used to calculate the error for that grid box.

An ensemble of integrations from the same three initial conditions previously used was done using the USGS SiB map with all the SiB vegetation type 12 points over the U.S. (Plate 1b) replaced with SiB vegetation type 2. Otherwise, the integrations in the ensemble were carried out in identical fashion to those in the USGS SiB map ensemble previously discussed. The new ensemble will hereafter be referred to as the TREE ensemble.

The TREE minus USGS SiB map ensemble difference in evaporation for June, July, August, and JJA is shown in Fig. 6a–d, respectively. A significant and large (1–2 mm/d) positive evaporation difference occurs over the central and eastern U.S. during July and August, and significant, though lesser positive differences occur during June and JJA. These evaporation differences are centered over the region of crop vegetation type in the USGS SiB map (Plate 1b). It is important to note that this region is west of the region where trees replaced crops in the experiment described in the last section (USGS vs. OLD SiB map). This is important because of the strong zonal gradient of the mean soil wetness, and the larger impact of vegetation anomalies in less than saturated conditions (here), as opposed to saturated conditions (farther east in previous experiment).

The TREE minus USGS SiB map ensemble difference in surface air temperature for June, July, August, and JJA is shown in Fig. 7a–d, respectively. An area of significant, large negative surface temperature differences (up to 6°C) closely corresponds in both magnitude and extent to the area of positive evaporation differences noted above. The large region of negative

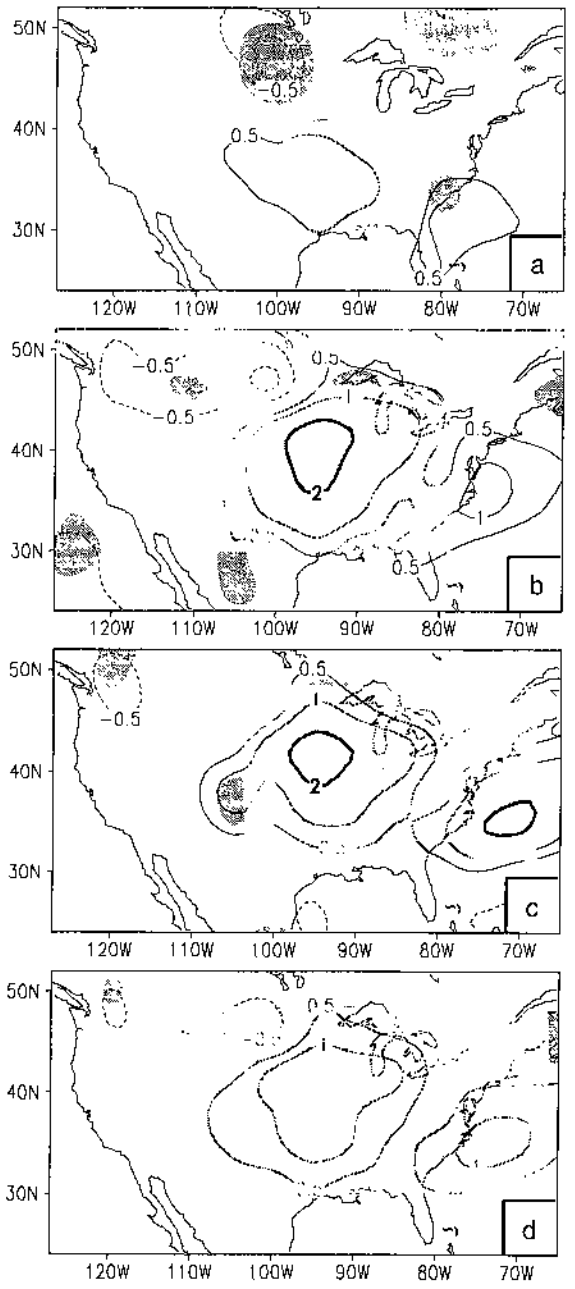

FIG. 6. TREE SiB map minus USGS SiB map ensemble difference in evaporation for (a) June, (b) July, (c) August, and (d) JJA (June-July-August mean). Contours show differences in mm/d. Dashed contours are negative. Areas with statistically significant differences are denoted by shading.

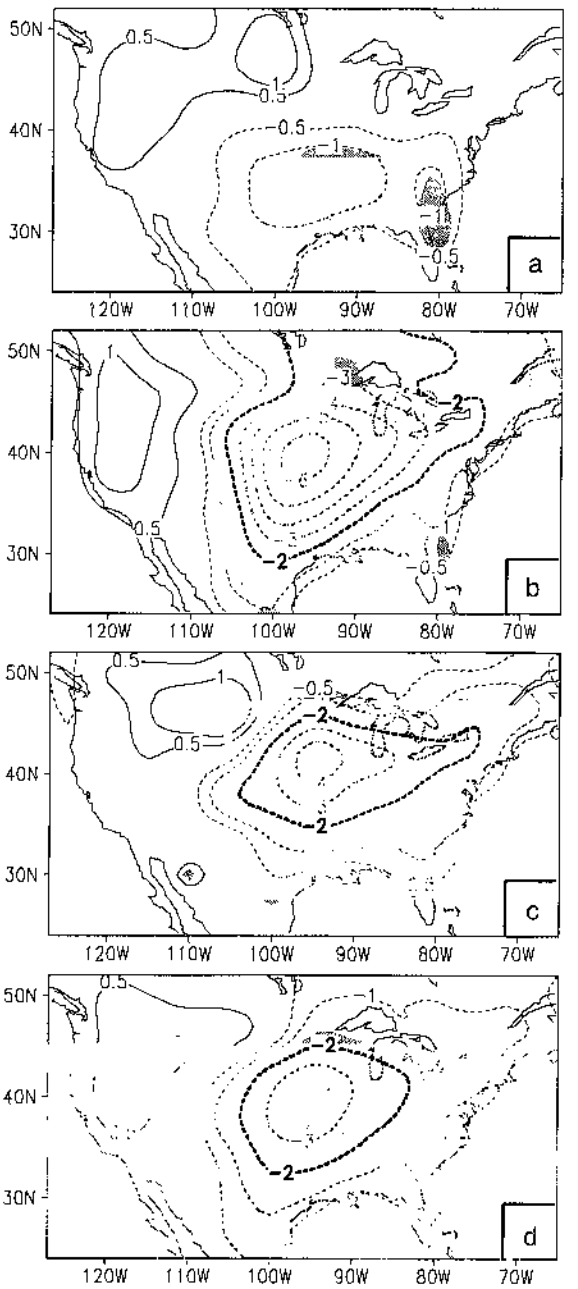

FIG. 7. TREE SiB map minus USGS SiB map ensemble difference in surface air temperature for (a) June, (b) July, (c) August, and (d) JJA (June-July-August mean). Contours show differences in °C. Dashed contours are negative. Areas with statistically significant differences are denoted by shading.

differences of up to 3°C over the central U.S. in the JJA mean (Fig. 9d) is well situated to correct much of the model surface temperature error in the U.S. region (Fig. 5a).

The TREE minus USGS SiB map ensemble difference in precipitation for June, July, August, and JJA is shown in Fig. 8a–d, respectively. Again the precipitation differences display more month-to-month variability and less significance than either the evaporation or surface temperature differences. However there is a persistent positive precipitation difference over the central and eastern U.S., which is coincident and consistent with the evaporation and surface temperature differences. The JJA mean positive 0.5–1 mm/d difference over the central U.S. and negative 0.5 mm/d

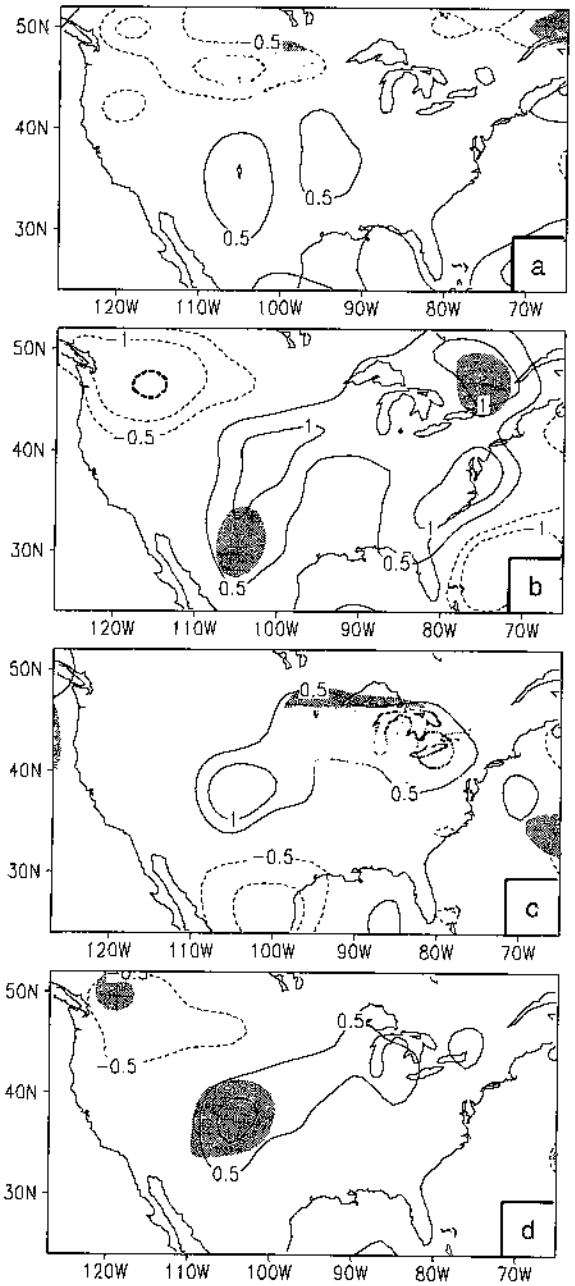

FIG. 8. TREE SiB map minus USGS SiB map ensemble difference in precipitation for (a) June, (b) July, (c) August, and (d) JJA (June-July-August mean). Contours show differences in mm/d. Dashed contours are negative. Areas with statistically significant differences are denoted by shading.

difference over the northwestern U.S. (Fig. 8d) would both contribute to reducing the model JJA mean precipitation errors (Fig. 5b).

Because the negative surface temperature differences and positive precipitation differences over the central U.S. (Figs. 7d and 8d) are negatively correlated with the model systematic errors (Fig. 5a, b), it is possible that the model systematic errors in this region are indeed related to the SiB crop vegetation type. As the latest available data have been used to determine the areal extent of the vegetation types in the USGS SiB vegetation map, it is likely that the model errors are related to the parameters used to specify the crop vegetation type, rather than to the use of an incorrect vegetation map. There is a strong seasonality (time variation due to the seasonal cycle) in the parameters used to describe the SiB crop vegetation type. This seasonality is designed to represent the different stages in the growth cycle of the crops. The values of these parameters were derived from field data obtained from sites with winter wheat (Dorman and Sellers 1989). Recent research has indicated that the seasonality in these parameters is inappropriate for application to all conterminous U.S. summertime crops (Xue et al. 1996). The seasonality of the natural deciduous tree vegetation substituted for the crops in this experiment is much weaker, and may be more appropriate. This seasonality is both different and considerably weaker than that of the crop vegetation type.

CONCLUSIONS

The COLA GCM, which is a global atmospheric model coupled to the SSiB model, has been used to test the sensitivity of boreal summer simulations over the U.S. to the vegetation prescribed. A new SiB vegetation map for the U.S. based on 1990 satellite and surface observations has been created by USGS. Significant differences in both monthly and seasonal simulations of evaporation, surface air temperature, and precipitation were obtained when the new USGS SiB vegetation map was used.

The COLA GCM boreal summer simulations over the U.S. contain systematic errors in the surface temperature and precipitation fields, which appear related to the SiB crop vegetation type. These errors are likely related to the use of vegetation parameters in the SiB crop vegetation type, which include seasonality, which is inappropriate for application to all U.S. summertime crops. To correctly specify the vegetation parameters and their seasonality a thorough analysis of the appropriate field data is required. This is a subject of further research by the authors.

Although the importance of specific vegetation parameters may be model dependent, the results of the experiments presented here underlie the importance of correctly specifying the correct vegetation types and the correct vegetation parameters for monthly and seasonal predictions over the U.S.

ACKNOWLEDGMENTS

The authors would like to thank L. Steyaert and T. Loveland of USGS for initiating and supporting this project and for providing the USGS SiB vegetation map. We would also like to thank J. Janowiak for his help and advice concerning the CAMS station precipitation and surface temperature data and R. Reynolds for providing the sea surface temperature data.

This work was conducted under support from the National

Science Foundation (NSF) and the National Oceanic and Atmospheric Administration (NOAA) through NSF grants ATM-93-41271 and NOAA grant NA46GP0340-02. Computational support was provided by the NASA Center for Computational Sciences.

Literature Cited

Alpert, J. C., M. Kanamitsu, P. M. Caplan, J. G. Sela, H. H. White, and E. Kalnay. 1988. Mountain induced gravity wave drag parameterization in the NMC medium-range forecast model. Pages 726–733 *in* Proceedings of the Eighth Conference on Numerical Weather Prediction. American Meteorological Society, Baltimore, Maryland, USA.

Anthes, R. A. 1977. A cumulus parameterization scheme utilizing a one-dimensional cloud model. Monthly Weather Review **105**:270–300.

Businger, J. A., J. C. Wyngaard, Y. I Zumi, and E. G. Bradley. 1971. Flux-profile relationships in the atmosphere surface layer. Journal of Atmospheric Science **28**:181–189.

Camillo, P. J., and R. J. Gurney. 1986. A resistance parameter for bare-soil evaporation models. Soil Science **2**:95–105.

Charney, J. G., W. J. Quirk, S. H. Chow, and J. Kornfield. 1977. A comparative study of the effects of albedo change on drought in semi-arid regions. Journal of Atmospheric Science **34**:1366.

Davies, R. 1982. Documentation of the solar radiation parameterization in the GLAS Climate Model. National Aeronautic and Space Administration Technical Memorandum **83961**.

Dickinson, R. E., and A. Henderson-Sellers. 1988. Modelling tropical deforestation: a study of GCM land-surface parameterization. Quarterly Journal of the Royal Meteorological Society **114**:439–462.

Dickinson, R. E., A. Henderson-Sellers, P. J. Kennedy, and M. F. Wilson. 1986. Biosphere–Atmosphere Transfer Scheme (BATS) for the NCAR Community Climate Model. National Center for Atmospheric Research Technical Note 275+STR. Climate and Dynamics Division, National Center for Atmospheric Reasearch, Boulder, Colorado, USA.

Dorman, J. L., and P. Sellers. 1989. A global climatology of albedo, roughness length and stomatal resistance for atmospheric general circulation models as represented by the Simple Biosphere Model (SiB). Journal of Applied Meteorology **28**:833–855.

Fennessy, M. J., J. L. Kinter III, B. Kirtman, L. Marx, S. Nigam, E. Schneider, J. Shukla, D. Straus, A. Vernekar, Y. Xue, and J. Zhou. 1994. The simulated Indian monsoon: a GCM sensitivity study. Journal of Climate **7**:33–43.

Goodchild, M. F., B. O. Parks, and L. T. Steyaert. 1993. Environmental modeling with GIS. Oxford University Press, Oxford, UK.

Harshvardhan, R. Davies, D. A. Randall, and T. G. Corsetti. 1987. A fast radiation parameterization for general circulation models. Journal of Geophysical Research **92**: 1009–1016.

Hou, Y.-T. 1990. Cloud-radiation-dynamics interaction. Dissertation. University of Maryland, College Park, Maryland, USA.

Jarvis, P. G. 1976. The interpretation of the variations in leaf water potential and stomatal conductance found in canopies in the field. Philosophical Transactions of the Royal Society of London Series B **273**:593–610.

Kinter, J. L., III, J. Shukla, L. Marx, and E. K. Schneider. 1988. A simulation of the winter and summer circulations with the NMC global spectral model. Journal of Atmospheric Science **45**:2486–2522.

Kuchler, A. W. 1983. World map of natural vegetation. Pages 16–17 *in* Goode's world atlas. Sixteenth edition. Rand Mcnally, New York, New York, USA.

Kuo, H. L. 1965. On formation and intensification of tropical cyclones through latent heat release by cumulus convection. Journal of Atmospheric Science **22**:40–63.

Lacis, A. A., and J. E. Hanson. 1974. A parameterization for the absorption of solar radiation in the earth's atmosphere. Journal of Atmospheric Science **32**:118–133.

Loveland, T. R., J. W. Merchant, D. O. Ohlen, and J. F. Brown. 1991. Development of a land-cover characteristics database for the conterminous U.S. Photommetric Engineering and Remote Sensing **57**:1453–1463.

Matthews, E. 1984. Prescription of land-surface boundary conditions in GISS GCM II: a simple method based on high-resolution vegetation data bases. National Aeronautic and Space Administration Technical Memorandum **86096**.

Mellor, G. L., and T. Yamada. 1982. Development of a turbulence closure model for geophysical fluid problems. Reviews in Geophysics and Space Physics **20**:851–875.

Mintz, Y. 1984. The sensitivity of numerically simulated climates to land-surface conditions. Pages 79–105 *in* J. Houghton, editor. The global climate. Cambridge University Press, Cambridge, UK.

Paulson, C. A. 1970. Mathematical representation of wind speed and temperature profiles in the unstable atmospheric surface layer. Journal of Applied Meteorology **9**:857–861.

Reynolds, R. W. 1988. A real-time global sea surface temperature analysis. Journal of Climate **1**:75–86.

Ropelewski, C. F., J. E. Janowiak, and M. F. Halpert. 1985. The analysis and display of real time surface climate data. Monthly Weather Review **113**:1101–1107.

Sela, J. G. 1980. Spectral modeling at the National Meteorological Center. Monthly Weather Review **108**:1279–1292.

Sellers, P. J. 1985. Canopy reflectance, photosynthesis and transpiration. International Journal of Remote Sensing **6**: 1335–1372.

Sellers, P. J., Y. Mintz, Y. C. Sud, and A. Dalcher. 1986. A simple biosphere model (SIB) for use within general circulation models. Journal of Atmospheric Science **43**:505–531.

Shukla, J., and Y. C. Mintz. 1982. Influence of land-surface evapotranspiration on the earth's climate. Science **215**: 1498–1501.

Slingo, J. M. 1987. The development and verification of a cloud prediction scheme for the ECMWF model. Quarterly Journal of the Royal Meteorological Society **103**:29–43.

Sud, Y. C., and M. J. Fennessy. 1982. A study of the influence of surface albedo on July circulation in semi-arid regions using the GLAS GCM. Journal of Climatology **2**:105–125.

Sud, Y. C., and W. E. Smith. 1985. The influence of surface roughness of deserts on the July circulation. Boundary-Layer Meteorology **33**:15–40.

Tiedtke, M. 1984. The effect of penetrative cumulus convection on the large-scale flow in a general circulation model. Contributions to Atmospheric Physics **57**:216–239.

Walker, J. M., and P. R. Rowntree. 1977. The effect of soil moisture on circulation and rainfall in a tropical model. Quarterly Journal of the Royal Meteorological Society **103**: 29–46.

Xue, Y., M. J. Fennessy, and P. J. Sellers. 1996. Impact of vegetation properties on U.S. summer weather prediction. Journal of Geophysical Research **101**:7419–7430.

Xue, Y., and P. J. Sellers. 1993. A brief review of the simple biosphere model. Pages 290–295 *in* M. F. Goodchild, B. O. Parks, and L. T. Steyaert, editors. Environmental modeling with GIS. Oxford University Press, Oxford, UK.

Xue, Y., P. J. Sellers, J. L. Kinter, III, and J. Shukla. 1991. A simplified biosphere model for global climate studies. Journal of Climate **4**:345–364.

Xue, Y., and J. Shukla. 1993. The influence of land surface properties on Sahel climate. Part I: desertification. Journal of Climate **6**:2232–2245.